IMAGE INFORMATICS APPROACHES TO ADVANCE CANCER DRUG DISCOVERY

Scott J. Warchal

Doctor of Philosophy
The University of Edinburgh
2018

DECLARATION

This thesis presents my own work, and has not been submitted for any other degree or professional qualification. Wherever results were obtained in collaboration with others, I have clearly stated it in the text. Any information derived from the published work of others has been cited in the text, and a complete list of references can be found in the bibliography. Published papers arising from the work described in this thesis can be found in the appendices.

– Scott Warchal, 2018

epigraph here

ACKNOWLEDGEMENTS

Acknowledgements here.

ABSTRACT

Abstract here.

LAY SUMMARY

Lay summary here.

CONTENTS

LIST OF FIGURES

LIST OF TABLES

LIST OF ACRONYMS

2D Two-dimensional

3D Three-dimensional

ANN Artificial neural network

BSA Bovine serum albumin

CNN Convolutional neural networks

DMEM Dulbecco's modified eagle medium

DMSO Dimethyl sulfoxide

EMA European Medicines Agency

FDA U.S Food and Drug Administration

GPU Graphics processing unit

HTS High throughput screening

MOA Mechanism of action

PBS Phosphate buffered saline

PCA Principal component analysis

PDD Phenotypic drug discovery

RGB red green blue

SAR Structure activity relationship

TCCS Theta comparative cell scoring

1 INTRODUCTION

1.1 Eroom's Law: The increasing cost of drug discovery

Throughout the last 70 years the cost of developing a new drug has steadily increased. A study by Scannel *et al.* noted the cost to develop a new drug has approximately doubled every 9 years[1], this observation has been dubbed "Eroom's law", a homage to Moore's law – the well-known observation that the number of transistors in microprocessors approximately doubles every 2 years. The cost of bringing a new drug to market is now approaching £1 billion, taking 10 years from initial concept to approval, the reasons behind this every-increasing cost are still very much in debate, though most agree the issue is multi-faceted. One explanation may be that the low-hanging fruit has been taken, effective traditional remedies have been studied and their active ingredients commercialised, natural products screened, leaving us to tackle the more complex diseases and pharmacological targets. This pessimism has led to the ever present idea that drug discovery is undergoing a productivity crisis, and that the investments made in early stage research do not translate into actionable pharmacology which can be used to develop efficacious therapies and ultimately benefit patients. This belief has led to a renewed interest in alternative drug discovery paradigms.

1.2 The drug discovery process

1.2.1 Target-based screening

Over the past 30 years the majority of drug discovery programmes have seized upon technological advances in robotics and automation to screen ever expansive compound libraries against predefined protein targets. It would be difficult to argue that this target-based high-throughput screening (HTS) approach has not been fruitful, yielding many succesful therapeutics across a range of disease areas, largely attributed to an increased understanding of the genomic basis of many diseases. However, despite numerous clinical and commerical success stories, HTS is not a panacea, with a high attrition rate of lead compounds once they enter clincial trials**citation_needed**. A large majority of these clinical trial failures are not due to toxicity, but rather a lack of efficacy which can often be traced back to a poorly hypothesised target in the face of complex disease aetiology.

1.2.2 Phenotypic screening

Phenotypic screening differs from target-based screening in that it does not rely on prior knowledge of a specific target, but instead interrogates a biologically relevant assay to identify compounds

which alter the phenotype in a biologically desirable way. This target-agnostic approach can prove useful in diseases with poorly understood mechanisms, or those with no obvious druggable protein targets. Phenotypic screening is not a new approach in small molecule drug discovery, it was the primary method for many decades before the genomics revolution made target hypothesis tractable**Zheng2013**.

An example of a modern day target-agnostic phenotypic screen is the development of the anti-hepatitis C drug daclatasvir. A model was developed in which human cells were modified to express the hepatitis C virus (HCV) replicon, this was then screened to identify compounds which reduced HCV replication. The target for daclatasvir was later found to be the HCV NS5A protein, which is a novel target and likely not have been suggested in a hypothesis-driven screen as at the time it was thought to have no involvement with HVC.[2,3]. This elegant assay has the very useful attribute of modelling the disease whilst simulatenously identifying compounds which may prove to be toxic in human cells.

Many concerns related to phenotypic screening are centered on the lack of mechanistic information for a given lead compound. Whilst the lack of a known target may cause concerns within a commercial drug discovery programme, regulatory bodies such as the Food and Drug Administration (FDA) and European Medicines Agency (EMA) do not require a known target for drug approval – only that it is safe and efficacious. Metformin, a first-line therapy for type 2 diabetes, and is on the World Health Organisation's list of essential medicine, decreases liver glucose production and has a insulin senstitising effect on many tissues. Despite approval in Europe since 1957 and widespread clinical use, the molecular mechanism of metformin remained unknown for 43 years[4]. Although knowledge of the molecular target is not necessary to get a drug into the clinic, target deconvolution is still an important part of phenotypic drug discovery programmes. Without knowing which protein or proteins a compound is binding to, lead optimisation via structure activity relationship (SAR) studies becomes extremely difficult. In addition, knowledge of the molecular target of a lead compound generated by a phenotypic screen can be used as a basis for starting a more high-throughput hypothesis-driven screen on a novel target. It is for this reason that many view phenotypic screening as a complimentary method to target based screening, rather than a competing approach or a proposed replacement.

1.3 High content imaging

High content imaging is a technique utilising high-throughput microscopes and automated image analysis, commonly used in phenotypic screening as a method for gathering multivariate datasets from images of biological specimens and has proven useful in a wide variety of phenotypic assays, ranging from 2D mammalian cells**cite_HCA_cell_papers**, *in vivo* studies in zebrafish[5] and even plants and crops[6].

High content screens – screening studies carried out with high content imaging – are particularly useful in phenotypic drug discovery for a few reasons. The first is that they allow the use of more complicated assays, which might better represent the biological complexity than simple reductionist models. However, these complex assays often have readouts which are more difficult to quantify,

Cell line	Molecular subclass	Mutational status PTEN	PI3K
MCF7	ER	WT	E545K
T47D	ER	WT	H1047R
MDA-MB-231	TN	WT	WT
MDA-MB-157	TN	WT	WT
HCC1569	HER2	WT	WT
SKBR3	HER2	WT	WT
HCC1954	HER2	⋆	H1047R
KPL4	HER2	⋆	H1047R

Table 1.1: Panel of breast cancer cell lines chosen for study. PI3K:Phosphoinsitide-3-kinase, PTEN:Phosphatase and tensin homolog, ER:Estrogen receptor, TN:triple-negative, HER2:human epidermal growth factor, WT:wild-type, ⋆:lack of consensus regarding the mutational status.

which a single univariate readout may fail to accurately recapitulate, therefore the multivariate datasets produced by high content screening enables a more detailed representation of a complex assay endpoint. A second benefit is that the multivariate nature of the data generated by high content screening facilitates a more unbiased method for selecting hits.

1.4 Cancer drug discovery

Cancer drug discovery programmes of past decades seized upon uncontrolled proliferation as a clinically relevant phenotype to screen against, giving rise a number of cytotoxic anti-proliferative and cytotoxic compounds, often renowned for their severe side-effects. Many modern day oncology drug discovery programmes still retain anti-proliferation as a key marker for pre-clinical success, although our ever increasing knowledge of cancer's molecular underpinnings has driven many oncology programmes towards a more target-based approach. The prototypical success story of target-driven drug discovery in oncology is imatinib, a tyrosine kinase inhibitor targetting the bcr-abl fusion protein in chronic myeloid leukemia. However, despite imatinib's success, in most cases targeting a single driver in a complex signalling network results in compensatory signalling, activation of redundant pathways, and unpredicted feedback mechanisms which often diminish or completely amilerorate efficacy *in vivo*.

2 CELL MORPHOLOGY CAN BE USED TO PREDICT COMPOUND MECHANISM-OF-ACTION

2.1 Introduction

Cellular morphology is influenced by multiple intrinsic and extrinsic factors acting on a cell, and striking changes in morphology are observed when cells are exposed to biologically active small molecules. This compound-induced alteration in morphology is a manifestation of various perturbed cellular processes, and we can hypothesise that compounds with similar MoA which act upon the same signalling pathways will produce comparable phenotypes, and that cell morphology can, in turn, be used to predict compound MoA.

In 2010 Caie *et al.* generated, as part of a larger study, an image dataset consisting of MCF7 breast cancer cells treated with 113 small molecules grouped into 12 mechanistic classes, these cells were then fixed, labelled and imaged in three fluorescent channels[7]. This dataset (also known as BBBC021) has become widely used as a benchmark in the field for MoA classification tasks, with multiple publications using the images to compare machine learning and data pre-processing approaches[8,9,10,11]. Whilst this is important work, it has led to the situation whereby the vast majority of studies in this field have based their work on a single dataset generated with a one cell-line.

One of the issues associated with phenotypic screening when used in a drug discovery setting is target deconvolution. Once a compound has been identified which results in a desirable phenotype in a disease-relevant assay it is common to want to know which molecular pathways the hit compound is acting upon. While target deconvolution is a complex and difficult task, image-based morphological profiling represents one option similar to transcriptional profiling that can match and unknown compound to the nearest similar annotated compound in a dataset, while at the same time being far cheaper than the transcriptional methods such as LINCS1000[12].

2.2 Creating an annotated dataset

As part of a preliminary study, a dataset similar to that of Caie *et al.*'s was generated consisting of 24 compounds grouped into 8 mechanistic classes screened across the panel of 8 breast cancer cell-lines (see table 1.1)

Compound	MoA class	Supplier	Catalog no.
Paclitaxel	Microtubule disrupting	Sigma	T7402
Epothilone B	Microtubule disrupting	Selleckchem	S1364
Colchicine	Microtubule disrupting	Sigma	C9754
Nocodazole	Microtubule disrupting	Sigma	M1404
Monastrol	Microtubule disrupting	Sigma	M1404
ARQ621	Microtubule disrupting	Selleckchem	S7355
Barasertib	Aurora B inhibitor	Selleckchem	S1147
ZM447439	Aurora B inhibitor	Selleckchem	S1103
Cytochalasin D	Actin disrupting	Sigma	C8273
Cytochalasin B	Actin disrupting	Sigma	C6762
Jaskplakinolide	Actin disrupting	Tocris	2792
Latrunculin B	Actin disrupting	Sigma	L5288
MG132	Protein degradation	Selleckchem	S2619
Lactacystin	Protein degradation	Tocris	2267
ALLN	Protein degradation	Sigma	A6165
ALLM	Protein degradation	Sigma	A6060
Emetine	Protein synthesis	Sigma	E2375
Cycloheximide	Protein synthesis	Sigma	1810
Dasatinib	Kinase inhibitor	Selleckchem	S1021
Saracatinib	Kinase inhibitor	Selleckchem	S1006
Lovastatin	Statin	Sigma	PHR1285
Simvastatin	Statin	Sigma	PHR1438
Camptothecin	DNA damaging agent	Selleckchem	S1288
SN38	DNA damaging agent	Selleckchem	S4908

Table 2.1: Annotated compounds and their associated mechanism-of-action label used in the classification tasks.

2.2.1 Compounds

The 24 compounds see table 2.1 were chosen based on previous knowledge of their biological activity and wide range of morphological responses, most of the compounds feature in Caie *et al.*s original dataset.

2.2.2 Cell painting: labelling cellular morphology

In order to capture a broad view of morphological changes within a cell using fluorescent microscopy, a choice has to be made which cellular structures to label. This choice is limited by the availablity of the fluorescent filter sets fitted to the microscope, reagent costs, and the scalability of the protocol when used in a large screen. Fortunately, this problem was already addressed by another group who published a protocol – named "cell painting" – for labelling 7 cellular structures, using 6 non-antibody stains imaged in the same 5 fluorescent channels available with our miscoscopy setup[13,14].

The cell-painting protocol was initially optimised by Gustafsdottir *et al.* for use in the U2OS oesteosarcoma cell line, and briefly tested in a few other commonly used cell-lines. However, when tested on the panel of 8 breast cancer cell lines, the staining protocol was observed to induce morphological changes on certain cell lines, in the absence of compounds. It was found that changing the media, and adding the MitoTracker DeepRed stain to live MDA-MB-231 cells produced a rounded morphology, which was not observed in the other cell lines. As any morpholgical changes

Stain	Labeled Structure	Wavelength (ex/em [nm])	Concentration	Catalog no.; Supplier
Hoechst 33342	Nuclei	387/447 ±20	2 μg/mL	#H1399; Mol. Probes
SYTO14	Nucleoli	531/593 ±20	3 μM	#S7576; Invitrogen
Phalloidin 594	F-actin	562/624 ±20	0.85 U/mL	#A12381; Invitrogen
Wheat germ agglutinin 594	Golgi and plasma membrane	562/624 ±20	8 μg/mL	#W11262; Invitrogen
Concanavalin A 488	Endoplasmic reticulum	462/520 ±20	11 μ/mL	#C11252; Invitrogen
MitoTracker DeepRed	Mitochondria	628/692 ±20	0.6 μM	#M22426; Invitrogen

Table 2.2: Reagents used in the cell painting protocol and the excitation/emission wavelengths of the filters used in imaging. ex: excitation, em: emission

introduced by the staining protocol would mask those caused by small-molecules, the protocol was adapted by removing the media change step, and moving the addition of wheat germ agglutinin and MitoTracker DeepRed until after fixation. As the cells were now fixed immediately in their existing media this prevented any alterations to the morphology and improved the wheat germ agglutinin staining, although as the MitoTracker stain relies on membrane potential in mitochondria, the selectivity of the MitoTracker stain was reduced when used on fixed cells, though it still produced selective enough labelling to capture large changes in mitochondrial morphology.

2.3 Machine learning methods to classify compound MoA

Predicting compound MoA from phenotypic data is a classification task. This type of machine learning problem is well researched, and there are several models appropriate for our labelled data. As the raw data is in the form of images, it can approached as an image classification task, a problem in the field receiving lots of attention due to recent theoretical and technological breakthroughs. Whereas a more classical approach would be to extract morphological information from the images, generating a multivariate dataset from the images, and training a classifier on these morphological features.

To develop and validate a machine learning model the dataset has to be split into training, validation and test sets. This is because overfitting is a common problem in machine learning, whereby the model is trained and accurately predicts labels on one dataset, but performs poorly when applied to new data on which is was not trained. Most classifiction models will overfit to some degree, typically performing better on the training dataset than any other subsequent examples, but the challenge is to limit this overfitting, and also to ensure that the data used to report accuracy measures has not been used in any way to train or validate the model.

2.3.1 Comparison between classical and deep-learning machine learning methods

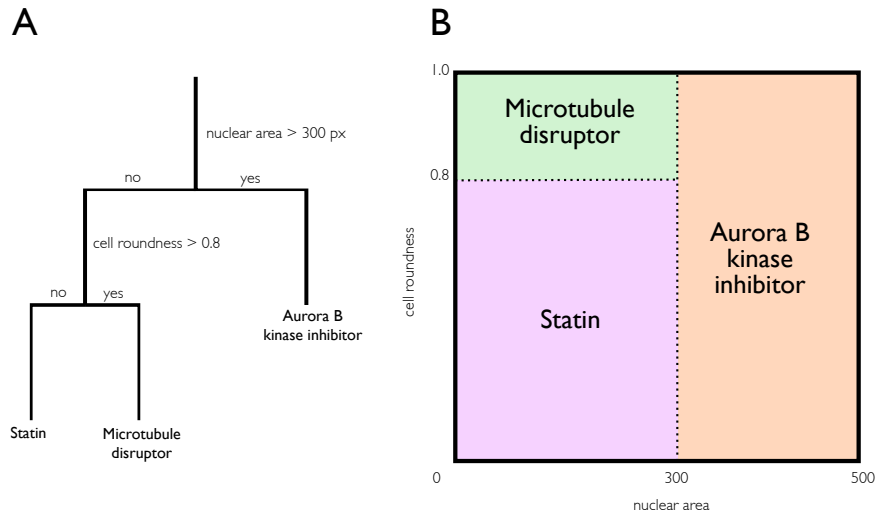

Figure 2.1: **(A)** An example of a simple mock decision tree to classify compound mechanism of action based on morphological features. **(B)** Depiction of decision space as divided by the decision tree model. Shaded areas show how new input data will be classified based on the decision rules (dotted lines).

Ensemble of decision trees trained on extracted morphological features

A decision tree is a very simple method that can be used for both regression and classification. The method works by repeatedly dividing the decision space using binary rules on the feature values until a terminal node containing a classification label is reached (figure 2.1). Simple decision trees like those shown in figure 2.1 perform relatively poorly on all but the simplest of classification problems. However, by aggregating many decision trees and their predictions we can create more accurate and robust models in a practice known as ensemble learning[15]. Bagging[16] and Boosting[17] are two popular methods for constructing ensembles of decision trees. As combining the output of several decision trees is useful only if there is a disagreement among them, these two methods both attempt to solve the same problem of generating a set of correct decision tress, that still disagree with one another as much as possible on incorrect predictions.

Decision tree methods work best with multivariate tabular data, with well defined features describing each observation, this is in contrast to image data which consists of 2D arrays of pixel intensities. Therefore, in order to train such a model, cellular morphology needs to be quantified by measuring cellular features. This is a common task with multiple software packages available, which follow two main steps: (1) Segment objects from the background. Objects may be subcellular structures or whole-cell masks (2) Measure various attributes from the object, this is typically based on size, shape and intensity. Cellprofiler[cellprofiler_paper] was chosen primarily due to the high configurability and the permissive license enabling large-scale distributed processing on compute clusters in order to reduce the image analysis time. The images captured on the ImageXpress were analysed using CellProfiler, quantifying approximately 400 morphological features. The datasets produced by the Cellprofiler analysis contained morphological measurements on an individual cell level. Although we can train a model on single cell data we are not interesting in classifying morphologies of single cells, but rather classifying an image or a collection of images

that represent a compound treatment, this therefore allows several approaches to structuring the training data:

1. Train and test on median profiles.
2. Train on single cell data, test on image or well median profiles.
3. Train on single cell data, test on single cell data and classify the parent image as the most commonly predicted class of cell in that image.
4. Train on median profiles of boostrapped single cell samples within an image, and test on median profiles.

Convolutional neural networks trained on pixel data

Artificial neural networks (ANNs) are becoming increasingly common in a wide range of machine learning tasks. Although many of the theories underpinning ANNs are decades old[perceptron_paper], they have only recently achieved widespread practical use due to improved methods for training[18] and the availability of more computing power allowing the use of more complex models. ANNs are (very) loosely inspired by the structure of biological brains, with interconnected neurons passing signals through layers onto subsequent neurons forming a chain with the output of one neuron becoming the input for the next neuron. In between neurons, the signals can be altered by multiplying the value by a weight (W), it is through adjusting these individual weights that ANNs optimise their performance for a particular task, similar to how long-term potentiation is used to strengthen synaptic connections in biological brains. When a signal reaches a neuron, it is combined via a weighted sum with all the other inputs from other connected neurons and passed through an activation function. This activation function – similar to an action potential in neurons – determines the output of the neuron for the given aggregated input, which is then passed as new inputs onto subsequent neurons and so on, however, in contrast to an all-or-nothing output of an action potential there are several types of activation functions used in ANNs, most of which have a graded output (figure 2.2B).

The neurons in an ANN are typically arranged in several layers: an input layer; one or more hidden layers; and a final output layer (figure 2.3). With each layer, the network transforms the data into a new representation, through training the network these representations make the data easier to classify. In the final layer, the data is ultimately represented in a way which makes a single output neuron activate more strongly than the other neurons in that layer, and so the data is ultimately transformed into a single value – the index of the active neuron which corresponds to a particular class. A new ANN is initialised with random weights, to train a neural network these weights are adjusted by feeding in labelled data and adjusting weights in order to minimise classification errors through a process known as backpropagation[18].

The convolution aspect of convolutional neural networks plays an important role when working with image data. Two-dimensional convolutions are widely used in image processing – blurring, sharpening and edge detection are all common operations which use this operation. They work by

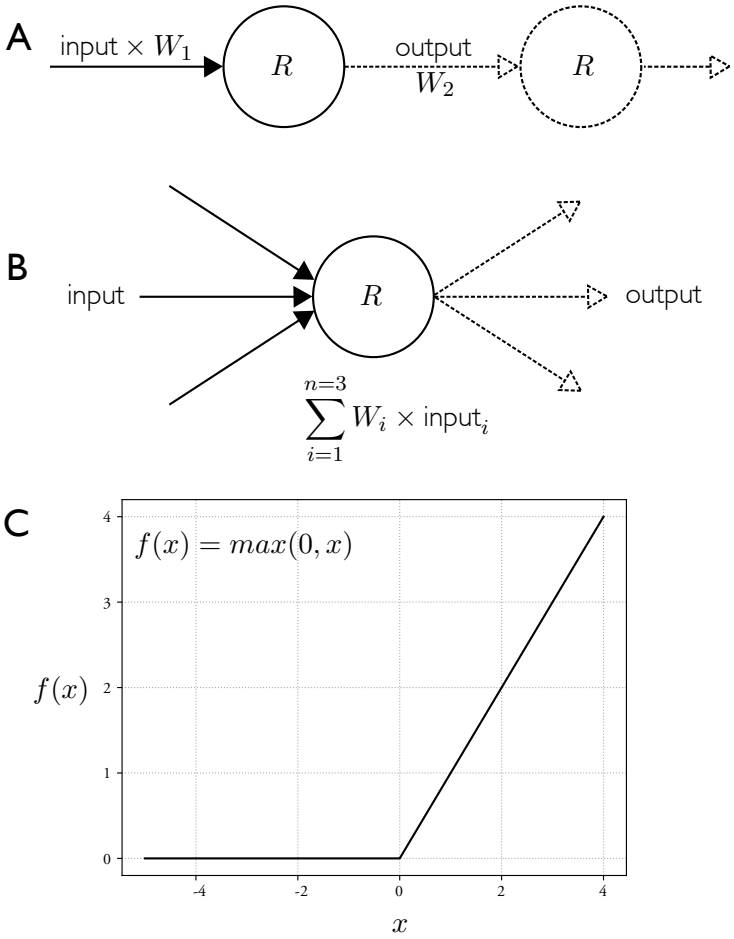

Figure 2.2: **(A)** A representation of a single connected neuron in an ANN, the input value to the neuron is multiplied by the weight (W_1), before being passed through the activation function R, the output of which is then multiplied by W_2, and passed as the input to the next neuron. **(B)** A neuron with multiple inputs and outputs, typical of those in a hidden layer. The activation function acts on the weighted sum of all inputs, and returns a single output value which is when directed to all connected neurons in the next layer. Where W_i is the weight of input_i. **(C)** A common activation function also known as a rectifier, in this example a rectified linear unit (ReLU), in the inputs (x) is transformed and passed as output. So $f(x)$ can be viewed as the output for a given value of x.

Figure 2.3 Representation of a simple 3-layer ANN with a single fully connected hidden layer, three input neurons and three output neurons. W denotes a weighted connection between an input neuron and a hidden-layer neuron, with all connections between neurons having an associated adjustable weight. A network such as this would take a vector of three numbers as input, and would be capable of predicting three classes from the output layer of three neurons depending on the activation strengths of the neurons in the final output layer.

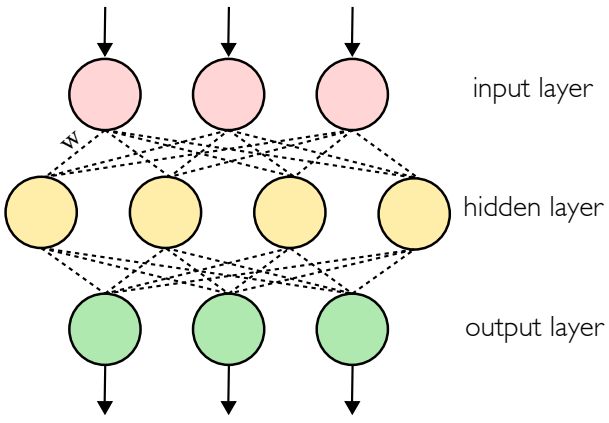

mapping a kernel – a smaller matrix of values – across a larger matrix, thereby using information from a small region of pixels in their transformation of each individual pixel. This lends itself well to ANNs, as a pixel value in isolation is less informative than a pixel value in the context of the neighbouring values. Depending on the size and the values within the kernel, the transformations highlight different features within an image. Two dimensional convolutions are used in ANNs by starting with many randomly initialised kernels, and updating the kernel values through training in order to best highlight features which prove useful for accurately predicting classes. Using a single convolutional layer highlights simple features in an image such as edges and speckles, by combining several convolutional layers more complex features are highlighted through combinations of these simple features. These convolved images are then flattened into a one-dimensional vector which is used as an input in an ANN such as that depicted in figure 2.3.

As CNNs can be constructed with a wide variety of architectures, and the field is still rapidly developing, I remained closed to well established architectures in the literature. However, as most images are digitially represented in three colour channels (red, green, blue (RGB)), the vast majority of CNN models are constructed in a way that input is restricted to three colour channels, therefore it is necessary to adapt these architectures to work with the differently shaped inputs and additional parameters generated by the 5 channel images generated with the ImageXpress.

The images generated by the ImageXpress microscope are 2160 by 2160 pixel tiff files, with a bit-depth of 16, whilst these image properties are common in microscopy, they are extreme for current CNN implementations. Most image classification tasks involving CNN's use 8-bit images in the region of 300 by 300 pixels, relatively small images are used as the convolutional layers of deep CNN's generate many thousands of matrices, and using smaller input images drastically reduces the computing resources and time required to train such classifiers.

This presents the issue of how to reduce the 2160×2160 images into small images, one option is to downscale the entire image using bi-linear or bi-cubic interpolation, while a second option is to chop the original image up into smaller sub-images (figure 2.4). Downsizing the original image by simple scaling has a few potential problems which make it unsuitable for this particular task: many of the finer-grained cell morphologies such as mitochondria and endoplasmic reticulum distribution will be lost due to the reduction in image resolution; in addition, it was found that whole well images are susceptible to over-fitting as the classfier learned biologically irrelevant features such as the locations of cells within an image, which although should be random might have some spurious association with particular class labels. When chopping images into sub-images the most simple and commonly used method is to chop each image into an evenly spaced grid, whilst this is unbiased and easy to implement, it has the downside of potentially returning many images that do not contain any cells. A more nuanced approach is to first detect the x,y co-ordinates of each in the image, and creating a 300×300 bounding-box around the centre of each cell. This method returns an image per cell, negating the issue of empty images; it does however require detecting cell locations and handling cells located next to the image border.

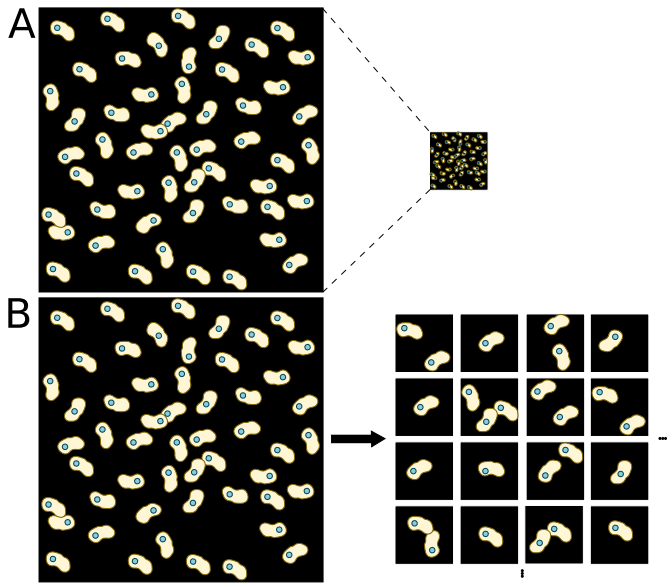

Figure 2.4: Two options for adapting large microscope images to work with the smaller input size of typical CNNs. **(A)** Full-sized images are downsized to the desired dimensions via bilinear or bicubic interpolation. **(B)** Images are chopped into smaller sub-images, cell detection can be carried out beforehand to ensure images contain at least one cell.

2.4 Predicting compound MoA on single cell lines

The first step is to determine a baseline of how well the predictive models perform when trained and tested on the same cell line, this also acts as a platform with which to test and optimise model architecture and hyperparameters.

The two different CNN architectures were tested based on the hypothesis that a deeper, more complex architecture (ResNet18[resnet_paper]) will be capable of learning more subtle features, although more complex models with greater numbers of interal parameters are more prone to overfitting when training data is limited. On the other hand, a more simple model such as AlexNet[alexnet_paper] which contains fewer convolutional layers will be less able to perform complex tranformations of the data, and therefore theoretically limit the subtle features which can be extracted and learned from an image. While this might theoretically reduce accuracy, in the absence of large amount of training data it may reduce overfitting due to the fewer number of parameters.

2.4.1 Ensemble of decision trees

2.4.2 CNNs

2.5 Transferring machine learning models to morphologically distinct cell lines

TODO: How well machine learning models generalise across cell-lines.

2.5.1 Leave-one-out classification

TODO.

2.5.2 Do additional cell-lines during training increase prediction accuracy?

TODO: When predicting MoA for a given cell-line, does adding additional training examples from other morphologically distinct cell-lines improve classification accuracy?

2.6 Discussion

TODO.

2.7 Methods

2.7.1 Cell culture

The cell-lines were all grown in DMEM (#CATNO MANUFACTURER) supplemented with 10% foetal bovine serum and 2 mM L-glutamine, incubated at 37°C, 5% CO_2. 2,500 cells were seeded into the inner 60 wells of optical bottomed 96-well plates (#165305 ThermoFisher) in 100 μL of media, whilst outer wells were filled with 100 μL of PBS.

After seeding with cells, assay plates were incubated for 24 hours prior to the addition of compounds.

2.7.2 Compound handling

Compounds (table 2.1) were diluted in DMSO at a stock concentration of 10 mM. Compounds plates were made in v-bottomed 96-well plates (#CATNO MANUFACTURER), at 1000-fold concentration in 100% DMSO by serial dilutions ranging from 10 mM to 0.3 μM in semi-log concentrations. Compounds were added to assay plates containing cells after 24 hours of incubation by first making a 1:50 dilution in media to create an intermediate plate, followed by a 1:20 dilution from intermediate plate to the assay plate, with an overall dilution of 1:1000 from the stock compound plate to the assay plate.

2.7.3 Staining

After 48 hours in the presence of compounds, assay plates were fixed by adding equal volume (100 μL) of 8% paraformaldehyde (#CATNO MANUFACTURER) to the existing media, resulting in a final paraformaldehyde concentration of 4%, and left to incubate at room temperature for 30 minutes. Wells were then washed with 100 μL of PBS and permeabilised with a 0.1% Triton-X100 solution for 20 minutes at room temperature. A cell-staining solution was made up in 1% bovine serum albumin (BSA) solution (see table 2.2). Wells were then washed again with 100 μL of PBS followed by addition of 30 μL staining solution. Plates were then incubated in the dark for 30 minutes at room temperature, washed 3 times with 100 μL of PBS. Before the final aspiration, plates were then sealed (#CATNO MANUFACTURER) and imaged.

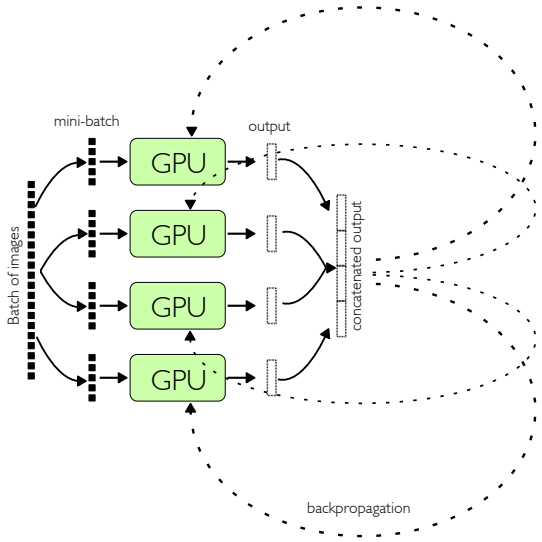

Figure 2.5: Increased training speed by data parallelism. Models are replicated across an array of GPUs, the input batch is split evenly among the devices, with each device processing a portion in parallel. During backpropagation the updated weights for all replicas are averaged and models weights are updated synchronously.

2.7.4 Imaging

Imaging was carried out on a multi-wavelength wide-field fluorescent microscope (ImageXpress micro XL, MolecularDevices, USA) with a robotic plate loader (Scara4, PAA, UK). Images were captured in 5 fluorescent channels (see table 2.2) at 20x magnification, exposure times were kept constant between plates and batches, as to not influence intensity values used in subsequent analyses.

2.7.5 Ensemble of decision trees

Models were created using scikit-learn version 0.19 in python 3.6.2.

2.7.6 Image analysis: numeric features from images

TODO

2.7.7 Convolutional neural networks

All code related to neural networks was written in pytorch (version 0.3) for python 3.5, and all ANN models were trained on Nvidia K80 GPUs. As training CNNs is computationally expensive and time consuming, data parallelism was leveraged to share batches of images across multiple GPUs. This technique replicates the CNN model on each device, which processes a portion of the input data, the updated weights for all devices are then averaged and model replicates are updated synchronously after each batch (figure 2.5). This speeds up model training approximately linearly with the number of GPUs and allows use of larger batch sizes.

Image preparation

TODO

3 MEASURING DISTINCT PHENOTYPIC RESPONSE

3.1 Section name

Random text before.

text text text here:

```
# example code highlighting
dist <- function(x) {
    return(sqrt(x %*% x))
}
```

Example text inbetween.

```
# some comment
def new_function(x):
    """docstring"""
    total = 0
    for i in x:
        total += 1
    return total
```

4 LARGE COMPOUND SCREEN ACROSS 8 BREAST CANCER CELL LINES

4.1 Section name

5 CHEMINFORMATICS

5.1 Section name

6 DISCUSSION AND CONCLUSION

6.1 Section name

BIBLIOGRAPHY

[1] Jack W Scannell, Alex Blanckley, Helen Boldon, and Brian Warrington. "Diagnosing the decline in pharmaceutical R&D efficiency". *Nature Reviews Drug Discovery* 11.March (2012), pp. 191–200.

[2] Makonen Belema and Nicholas A. Meanwell. "Discovery of daclatasvir, a pan-genotypic hepatitis C virus NS5A replication complex inhibitor with potent clinical effect". *Journal of Medicinal Chemistry* 57.12 (2014), pp. 5057–5071.

[3] James H. Nettles, Richard A. Stanton, Joshua Broyde, Franck Amblard, Hongwang Zhang, Longhu Zhou, Junxing Shi, Tamara R. McBrayer, Tony Whitaker, Steven J. Coats, James J. Kohler, and Raymond F. Schinazi. "Asymmetric binding to NS5A by daclatasvir (BMS-790052) and analogs suggests two novel modes of HCV inhibition". *Journal of Medicinal Chemistry* 57.23 (2014), pp. 10031–10043.

[4] Gerald I. Shulman Ripudaman S. Hundal, Martin Krssak, Sylvie Dufour, Didier Laurent, Vincent Lebon, Visnathan Chandramouli, Silvio E. Inzucchi, William C. Schumann, Kitt F. Petersen, Bernard R. Landau. "Mechanism by which metformin reduces glucose production in type 2 diabetes". *Diabetes* 49.12 (2000), pp. 2063–2069. arXiv: NIHMS150003.

[5] C Geoffrey Burns, David J. Milan, Eric J. Grande, Wolfgang Rottbauer, Calum A MacRae, and Mark C. Fishman. "High-throughput assay for small molecules that modulate zebrafish embryonic heart rate". *Nature Chemical Biology* 1.5 (2005), pp. 263–264.

[6] Dijun Chen, Kerstin Neumann, Swetlana Friedel, Benjamin Kilian, Ming Chen, Thomas Altmann, and Christian Klukas. "Dissecting the Phenotypic Components of Crop Plant Growth and Drought Responses Based on High-Throughput Image Analysis". *The Plant Cell Online* 26.12 (2014), pp. 4636–4655.

[7] Peter D Caie, Rebecca E Walls, Alexandra Ingleston-Orme, Sandeep Daya, Tom Houslay, Rob Eagle, Mark E Roberts, and Neil O Carragher. "High-content phenotypic profiling of drug response signatures across distinct cancer cells." *Molecular cancer therapeutics* 9.6 (2010), pp. 1913–26.

[8] V. Ljosa, P. D. Caie, R. ter Horst, K. L. Sokolnicki, E. L. Jenkins, S. Daya, M. E. Roberts, T. R. Jones, S. Singh, A. Genovesio, P. A. Clemons, N. O. Carragher, and A. E. Carpenter. "Comparison of Methods for Image-Based Profiling of Cellular Morphological Responses to Small-Molecule Treatment". *Journal of Biomolecular Screening* 18.10 (2013), pp. 1321–1329.

[9] S Singh, M Bray, T R Jones, and A E Carpenter. “Pipeline for illumination correction of images for high-throughput”. *Journal of Microscopy* 256.3 (2014), pp. 231–236.

[10] Nick Pawlowski, Juan C Caicedo, Shantanu Singh, Anne E Carpenter, and Amos Storkey. “Automating Morphological Profiling with Generic Deep Convolutional Networks”. *bioRxiv* (2016).

[11] D Michael Ando, Cory Y Mclean, and Marc Berndl. “Improving Phenotypic Measurements in High-Content Imaging Screens”. *bioRxiv* (2017).

[12] Qiaonan Duan, Corey Flynn, Mario Niepel, Marc Hafner, Jeremy L Muhlich, F Fernandez, Andrew D Rouillard, Christopher M Tan, Edward Y Chen, R Golub, Peter K Sorger, Aravind Subramanian, and Avi Ma. “LINCS Canvas Browser : interactive web app to query , browse and interrogate LINCS L1000 gene expression signatures”. *Nucleic acids research* 42.W1 (2014), W449–W460.

[13] Sigrun M Gustafsdottir, Vebjorn Ljosa, Katherine L Sokolnicki, J Anthony Wilson, Deepika Walpita, Melissa M Kemp, Kathleen Petri Seiler, Hyman a Carrel, Todd R Golub, Stuart L Schreiber, Paul a Clemons, Anne E Carpenter, and Alykhan F Shamji. “Multiplex cytological profiling assay to measure diverse cellular states.” *PloS one* 8.12 (2013), e80999.

[14] Mark-Anthony Bray, Shantanu Singh, Han Han, Chadwick T Davis, Blake Borgeson, Cathy Hartland, Maria Kost-alimova, Sigrun M Gustafsdottir, Christopher C Gibson, and Anne E Carpenter. “Cell Painting , a high-content image-based assay for morphological profiling using multiplexed fluorescent dyes”. *Nature Methods* 11.9 (2016), pp. 1757–1774.

[15] David W Opitz and Richard Maclin. “Popular Ensemble Methods: An Empirical Study”. *J. Artif. Intell. Res. (JAIR)* 11 (1999), pp. 169–198.

[16] Leo Breiman. “Bagging predictors”. *Machine Learning* 24.2 (1996), pp. 123–140.

[17] Yoav Freund and Robert E. Schapire. “Experiments with a New Boosting Algorithm”. *ICML’96 Proceedings of the Thirteenth International Conference on International Conference on Machine Learning*. 1996, pp. 148–156.

[18] David E. Rumelhart, Geoffrey E. Hinton, and Ronald J. Williams. “Learning representations by back-propagating errors”. *Nature* 323.6088 (1986), pp. 533–536.